This is a "preproof" accepted article for *Mineralogical Magazine*.
This version may be subject to change during the production process.
10.1180/mgm.2024.78

Hidden mineral treasures in rust samples of the Muonionalusta iron (IVA) meteorite

Alice Taddei[1], Dan Holtstam[2], Luca Bindi[1,3,*]

[1]Dipartimento di Scienze della Terra, Università degli Studi di Firenze, via La Pira 4, I-50121 Firenze, Italy

[2]Department of Geosciences, Swedish Museum of Natural History, Box 50007, SE-10405 Stockholm, Sweden

[3]CNR – Istituto di Geoscienze e Georisorse, sezione di Firenze, via La Pira 4, I-50121 Firenze, Italy

*Corresponding author: luca.bindi@unifi.it

Abstract

Exceptionally well-developed crystals of akaganeite, $(Fe^{3+},Ni^{2+})_8(OH,O)_{16}Cl_{1.25}\cdot nH_2O$, were observed during the investigation of rust samples from the Muonionalusta iron meteorite, constituting ideal candidates for the first single-crystal X-ray diffraction investigation carried out on this mineral. Other techniques here employed to study akaganeite include SEM-EDS and Raman spectroscopy.

https://doi.org/10.1180/mgm.2024.78 Published online by Cambridge University Press

The structure refinement ($R1$ = 2.31%) confirmed akaganeite to be monoclinic in symmetry (space group $I2/m$), with a = 10.560(4) Å, b = 3.0268(12) Å, c = 10.512(4) Å, β = 90.050(15)° and V = 336.0(2) Å^3. The mineral is also confirmed to be isostructural with monoclinic members of the hollandite supergroup, with 2 × 2 tunnels parallel to the b axis constituted by edge-linked Fe-octahedral chains. Chemical analyses resulted in a Cl range of 2.8–5.6 wt.% and an average mole Fe/Cl ratio of 7.6, with trace amounts of Si, Al and S (< 0.1 wt.%), and no detectable Ni or Co. The combination of structural and chemical data yielded the stoichiometric formula $Fe_8O_7(OH)_9Cl$. The Raman spectrum of the Muonionalusta akaganeite is comparable with Raman spectra from synthetic akaganeite, showing several peaks between 138 and 1390 cm^{-1} and the O–H stretching band at 3510 cm^{-1}; no peaks are observed in the H_2O bending-mode area of the spectrum, in keeping with the structural data. Taking into account all the collected data, we propose two possible new formulae for akaganeite (Z = 8): $FeO_{1-x}(OH)_{1+x}Cl_x$ ($0.01 < x < 0.20$) or, taking Ni into account, $(Fe_{1-x}Ni_x)O_{1-x-y}(OH)_{1+x+y}Cl_y$ ($0 < x < 0.19$ and $0.01 < y < 0.20$).

In the Muonionalusta corrosion rusts, besides akaganeite, also nickel-bearing humboldtine [$Fe(C_2O_4)\cdot 2H_2O$] was identified through Raman spectroscopy and chemical analyses. It possibly represents the first occurrence of an oxalate mineral as a product of terrestrial weathering of a meteorite.

Keywords: iron meteorite, terrestrial weathering, akaganeite, humboldtine, crystal structure, Raman spectroscopy, Muonionalusta

https://doi.org/10.1180/mgm.2024.78 Published online by Cambridge University Press

Introduction

Muonionalusta is an octahedrite that belongs to group IVA, which accounts for about 8% of all irons known. The primary mineralogy of the meteorite, with a Ni content of ~9 wt.% and 0.4 wt.% Co (Hidaka et al., 2019), has been described in detail elsewhere (Buchwald, 1975; Holtstam et al., 2003). The Muonionalusta meteoroid was disrupted from its parent world approximately 0.4 billion years ago in a violent impact event (Blichert-Toft et al., 2010). It descended to Earth in Middle Pleistocene, breaking up in the atmosphere and scattering over a large area (Lagerbäck and Wickman, 1997). The current distribution of meteorite fragments forms a disturbed strewn field spanning at least 25 × 15 km, with the main concentration found around Lake Kitkiöjärvi (lat. 67°49'N, long. 23°8'E, 255 m a.s.l.) in the Pajala District, Norrbotten, Sweden. Pieces ranging from 0.1 to 1200 kg can be found from near the surface down to at least 4 m in the soil.

The Quaternary deposits of this area consist primarily of till and postglacial accumulations of peat, though large sections are covered with glaciofluvial/lacustrine sediments (Fagerlind, 1981). It is inferred that meteorite fragments were moved by the ice sheet up to 8–20 km from the original impact site, based on the distribution pattern of hundreds of samples (Hättestrand, 2009). They have thus endured at least one glaciation, the Weichselian (115–12 k.y.), and thereafter, in a subpolar climate, they have been subjected to seasonal freeze-and-thaw cycles.

Muonionalusta meteorite samples are accompanied by a ‘rust crust’, consisting of various terrestrial alteration products, mainly Fe (±Ni) oxides and oxyhydroxides,

https://doi.org/10.1180/mgm.2024.78 Published online by Cambridge University Press

and relics of meteoritic minerals plus cemented soil particles (Wickman, 1964; Holtstam and Söderhielm, 2004; Gurdziel, 2012). Recent finds of muonionalustaite [$Ni_3(OH)_4Cl_2 \cdot 4H_2O$] (Holtstam et al., 2021) and parahibbingite [β-$Fe_2(OH)_3Cl$] (Margheri et al., 2022) have demonstrated a more diverse secondary mineralogy, emphasising the significance of chlorine in the terrestrial alteration processes.

In the current contribution, we present results from an investigation of akaganeite, $(Fe^{3+},Ni^{2+})_8(OH,O)_{16}Cl_{1.25} \cdot nH_2O$, and humboldtine, $Fe(C_2O_4) \cdot 2H_2O$, from meteorite rust samples, including the first single-crystal diffraction study of akaganeite and extended Raman spectroscopic data.

Materials and methods

Samples

Akaganeite crystals were taken from a small meteorite sample (~2 kg) found at 40 cm depth, 5 km NE of lake Kitiöjärvi. A second akaganeite sample (see also Margheri et al., 2022) used in the study is from a rust crust attached to a granitic cobble associated with a 22 kg meteorite specimen recovered from 1.4 m below the ground surface in the nearby area. The rust sample with humboldtine is from an unspecified meteorite find from ~60 cm depth.

Chemical analysis

The composition of the studied minerals was determined with spot analyses using a FEI Quanta 650 field-emission scanning electron microscope (SEM), fitted with an 80 mm^2 X-MaxN Oxford Instruments energy-dispersion (EDS) detector (operated at 20 kV, with beam size ~1 µm and at a working distance of 10 mm) on carbon-coated, polished samples. Beam current was calibrated on Co metal, with

https://doi.org/10.1180/mgm.2024.78 Published online by Cambridge University Press

the instrument calibrated against metal and mineral standards (including Fe and Ni metal, NaCl) for each element.

Single-crystal X-ray diffraction study of akaganeite

Several crystals were extracted from a cluster of pseudo-hexagonal, platy crystals and tested with single-crystal X-ray diffraction (SC-XRD). Among them, only one exhibited good diffraction quality. On this crystal, unit-cell parameters and intensity data were collected using a Bruker D8 Venture diffractometer equipped with a Photon III detector, with a graphite-monochromatized Mo*K*α radiation (λ = 0.71073 Å). Intensity data were corrected for absorption, using the multi-scan correction method (SADABS), and for Lorentz and polarisation effects with the APEX3 software suite (Bruker, 2016). Details of the data collection are listed in Table 1.

Structure refinement of akaganeite

The structure refinement was carried out in the space group *I*2/*m* using SHELXL (Sheldrick, 2015). Starting atomic positions were taken from Post and Buchwald (1991), with two Fe sites and four O sites located on a mirror plane (Wyckoff position 4*i*) and the Cl site positioned at the origin of the cell (Wyckoff position 2*a*). Scattering curves for neutral Cl, Fe and O were taken from the *International Tables for Crystallography* (Wilson, 1992). The Cl-site occupancy was refined and then fixed at the refined value; all the other sites were found to be fully occupied. Notably, the resulting Cl/Fe ratio obtained from the refinement, 0.123(1), is in good agreement with the value from chemical data, 0.13 (see below). Given a still very high *R*1 parameter (> 20%) at this stage, a non-

https://doi.org/10.1180/mgm.2024.78 Published online by Cambridge University Press

merohedral twinning was taken into account (matrix: |001/010/100|). The introduction of the twinning dramatically improved the refinement. Convergence was then achieved with an anisotropic model, with a final $R1$ = 2.23%. Lastly, residues in the ΔF map were examined in order to find the H atoms, but none of the attempts to include known hydrogen positions (see Post et al., 2003) led to satisfactory results.

Atomic coordinates and selected bond distances are listed in Table 2 and 3, respectively.

Raman spectroscopy

Raman spectra of both akaganeite and humboldtine were collected on a LabRAM HR 800 micro-spectrometer, with a 515 nm continuous-wave single-frequency diode pumped laser (Cobolt Fandango), a Peltier-cooled (−70°C) charge-coupled device detector (Synapse) and an Olympus MPlan N 100×/0.9 objective. The instrument was calibrated against the 521 cm^{-1} Raman band of silicon before sample measurements. Filters allowing laser throughput of 1% or 10% were employed, with laser spot on the sample surface being ~2 μm in diameter. The laser power on the samples for each filter was ~0.2 and ~2 mW, respectively. Instrument control and data acquisition (up to 500 s in 2 cycles with a 600 grooves/mm grating) were made with the LabSpec 6 software.

Results

Akaganeite

Akaganeite has been found as (A) large crystals, sometimes grouped in ‘rosettes’ (Figs 1, 2), and (B) as envelopes grown on parahibbingite crystals (Fig. 3; see also

https://doi.org/10.1180/mgm.2024.78 Published online by Cambridge University Press

Margheri et al., 2022). The single crystals are lustrous reddish brown and euhedral, with a (pseudo)hexagonal platy outline, and up to 1 mm across. They occur in cavities in a crust consisting of mainly fine-grained goethite and maghemite. Relics of unoxidised taenite lamellae and thin crusts of a greenish yellow, unknown Ni-(Fe)-Cl hydrate mineral also occur on the rust sample.

Chemical analyses (n = 35) of akaganeite (A) gave no detectable Ni or Co, traces of Si, Al, S (< 0.1 wt.% each). Cl ranges from 2.8 to 5.6 wt.% (average 4.4%; 1σ = 0.80). The average mole Fe/Cl ratio is 7.6. The sample (B; n = 6) is more homogeneous, with average Ni 1.3 wt.%, Co 0.6 wt.%; S 0.2 wt.%, Cl 7.5 wt.%; (Fe + Ni + Co)/Cl = 4.7. Whereas the minor Ni, Co, Si and Al are possibly substituting for Fe^{3+} in akaganeite, SO_4^{2-} ions may probably occupy space in the structural 'tunnels' (Peretyazhko et al., 2019).

For the Raman spectra of akaganeite, sample (B) (Fig. 4) produced the best result (highest peak-to-background and lower noise level). The spectrum was collected with the 1% filter, because the sample transformed with higher laser throughput. Although relative intensities vary (partly due to different excitation wavelengths of the lasers used in different studies), peak positions are in general good agreement (±7 cm^{-1}) with synthetic akaganeite (Oh et al., 1998; Rémazeilles and Refait, 2007; Li and Hihara, 2015), but previous studies show fewer observed bands in total and do not cover regions above 1000 cm^{-1} (including possible O–H vibration modes).

For akaganeite, the relatively weak 3510 cm^{-1} band is assigned to O–H stretching, and in sample (A) this band occurs at a close position, 3522 cm^{-1}. Both are compatible with a O···O–H distance > 3 Å (Libowitzky, 1999) as found from structural refinement.

https://doi.org/10.1180/mgm.2024.78 Published online by Cambridge University Press

Infra-red (IR) spectra of synthetic akaganeite powder show an absorption band at about 3485 cm^{-1}, ascribed to O–H stretching modes (Murad and Bishop, 2000), that may well correspond to the 3510 peak of the Raman spectrum. Another band of approximately equal strength at about 3390 cm^{-1} that is also reported from IR spectra (Murad and Bishop, 2000) has no counterpart in the Raman spectrum, although the background from 3300 to 3500 is slightly elevated here. The 3390 cm^{-1} band is assigned to OH–Cl interactions (Song and Boily, 2012).

Akaganeite is a thermally less stable mineral, known to transform to hematite or goethite depending on physical and chemical conditions (Ståhl et al., 2003; Fu et al., 2020). Raman recordings of akaganeite with a lower degree of filtering produced a distinct and reproducible result (Fig. 5) with well-defined peaks. The spectra obtained show no close resemblance to the common phases known in the Fe-O-(H) system. There is a very good match with data ascribed to synthetic nanoparticles of magnetite of about 20 nm in size (Yew et al., 2017), with bands at 212, 274, 388, 474, 585, and a broad feature at 1277 cm^{-1}. However, a more probable explanation is that their Fe_3O_4 oxidised to Fe_2O_3 under the laser beam, producing a pattern with red-shifted hematite Raman bands at high temperature, a phenomenon described by Shebanova and Lazor (2003). Our data, then, imply that temperatures at about 400°C were prevailing during analysis of akaganeite that unintentionally transformed into α-Fe_2O_3 with higher laser power.

The present material (A) was considered a good candidate for the first SC-XRD study of the species, because akaganeite forms exceptional (from outer morphology) and large crystals and has a negligible Ni content. The unit-cell parameters observed here (Table 1) are comparable to those found in previous structural studies, some of which employing neutrons and synchrotron radiation

https://doi.org/10.1180/mgm.2024.78 Published online by Cambridge University Press

on synthetic and natural powders (Post et al., 2003; Ståhl et al., 2003).

Humboldtine

Humboldtine was identified from powder X-ray diffraction, chemical analyses and Raman spectroscopy. It occurs in clusters, up to 0.5 mm wide (Fig. 6), of small, greenish yellow translucent crystals with complex morphology. They are found in a fragile, porous aggregate of mainly goethite, ferrihydrite and quartz + feldspar sand grains. The chemical data indicate solid solutions between humboldtine and its Ni-analogue, andreybulakhite (IMA no. 2023-037), with a range of atomic Fe/(Fe + Ni) values 0.77–0.51; average from 18 analyses is 0.60. No other metals were detected. The Raman spectrum (Fig. 7) is very similar to published data for humboldtine (Echigo and Kimata, 2008) and isotypic M^{2+} oxalate dihydrates (M = Mg, Mn, Fe, Ni, Zn; Giester et al., 2023). The intense band at 1470 cm^{-1}, related to C–O bending modes, can be compared with the corresponding Raman shift for the synthetic end-member Fe and Ni compounds, at 1463 and 1482 cm^{-1}, respectively. The band at 531 cm^{-1}, assigned to metal–O stretching, is apparently slightly moved (from pure Fe oxalate dihydrate at 523 cm^{-1}), probably related to the shorter average bond lengths in Ni-bearing humboldtine. It may be noted that, whereas the mineral was unstable under the electron beam of the SEM, there was no sample damage from the laser, not even for with the low-density filter (10%). Therefore, signals from vibrations of the H_2O molecules, manifesting O–H stretching at 3330 and bending at 1610 cm^{-1}, respectively, are clearly visible in the spectrum.

https://doi.org/10.1180/mgm.2024.78 Published online by Cambridge University Press

Discussion

Crystal structure details of akaganeite

The crystal symmetry of akaganeite was considered tetragonal until the early 1990s, when Post and Buchwald (1991) proposed the currently accepted monoclinic model. The SC-XRD diffraction data obtained in the present study are in excellent agreement with the latest literature data (Post and Buchwald, 1991; Post et al., 2003; Ståhl et al., 2003), thus confirming a monoclinic, *I*-centred crystal lattice.

Akaganeite, also known as β-FeOOH, is isostructural with monoclinic members of the hollandite supergroup (except hollandite *sensu stricto* and strontiomelane; Biagioni et al., 2013): the structure consists of double chains of edge-linked Fe octahedra that form 2 × 2 tunnels oriented along the *b* axis (Fig. 8).

Unlike hollandite-supergroup minerals, where the octahedrally coordinated sites are occupied by tetravalent cations (*i.e.* Ti^{4+}, Mn^{4+}), in the akaganeite structure they mostly host trivalent iron. When akaganeite forms in Ni-rich environments, *e.g.* when it occurs as weathering product of metal-bearing meteorites, Ni^{2+} can enter the octahedra at the expense of Fe^{3+} (Buchwald and Clarke, 1989; Post and Buchwald, 1991; Post et al., 2003), and the charge neutrality is kept by the addition of OH^- groups instead of O^{2-}. The sample (A) examined here seems to be an exception: despite being a secondary phase derived from the alteration of the Muonionalusta iron meteorite, it is devoid of nickel, leaving Fe^{3+} the only cation to occupy the octahedra (which is the case for 'terrestrial' akaganeites, *e.g.* Mackay, 1962; Holtstam, 2006). Fe^{3+} can be found at two distinct, distorted sites (Fe1 and Fe2) positioned slightly off-centre, possibly in order to minimise the cation-cation repulsion as occurs in other akaganeite samples (Post and Buchwald,

https://doi.org/10.1180/mgm.2024.78 Published online by Cambridge University Press

1991; Post et al., 2003) as well as in hollandite-supergroup minerals (*e.g.* Post et al., 1982). The distortion of the Fe2 octahedron is slightly more pronounced than that of Fe1. Both octahedra have three longer and three shorter distances, Fe1–O1 and Fe2–O3 being the longer ones (Table 3). This is expected, because hydrogen is bonded to O1 and O3 (Post et al., 2003): the longer Fe–O distances are due to a reduced effective charge for O in the hydroxyl group. The mean distances <Fe1–O> and <Fe2–O> are nearly identical to those presented by Post and Buchwald (1991). However, in the crystal studied here the bond distances range from 1.950 to 2.178 Å and from 1.941 to 2.211 Å, respectively. When compared to the values reported by Post and Buchwald (1991), these ranges appear fairly different, especially the Fe2–O one (1.80–2.32 Å in Post and Buchwald, 1991). This discrepancy could be explained by the improved accuracy of our data, considering that, in the aforementioned study, the pronounced difference in regularity between the two octahedra could not be explained and was attributed to a measurement artifact.

The site located at the centre of the tunnels is half-occupied by Cl^- anions, corresponding to 1 Cl atom per formula unit in the structural formula. In samples containing larger amounts of Cl (*e.g.* Post et al., 2003; Ståhl et al., 2003), where the tunnel site is occupied for two thirds, it has been observed that in order to have compatible Cl–Cl distances (~3.7 Å) the position of the site must slightly shift its position along the length of the tunnels. This is not necessary in the case of the studied crystal, because Cl ions could occupy every second site, thus not needing further separation from one another. Such an ordered configuration is in agreement with the relatively low thermal displacement parameter (0.043 $Å^2$), which roughly corresponds to about half of that observed by Post et al. (2003) in

https://doi.org/10.1180/mgm.2024.78 Published online by Cambridge University Press

the model involving the split Cl site (0.075 $Å^2$).

Formation of akaganeite

Akaganeite is a relatively common corrosion product of iron metal in natural environments, where there is a supply of Cl (Buchwald and Clarke, 1989; Bland et al., 2006; Holtstam, 2006). It is also a well-known component on some rusty archaeological artifacts (*e.g.* Selwyn et al., 1999) and as a product of steel corrosion (*e.g.* de la Fuente et al., 2011). Gurdziel (2012) has previously reported the occurrence of fine-grained akaganeite from Muonionalusta, but without detailed data. There are pedochemical factors to consider that promote formation of akaganeite here. The soils in this part of Sweden are exceptionally high in Cl, near 0.1%, which is related to weathering of scapolite- and apatite-group minerals in the regolith (Ladenberger et al., 2012). Experimental studies show that akaganeite can form at a wide range of pH (2–8) in Cl-rich environments, but is favoured at low pH (Peretyazhko et al., 2018). Values in soil (till) interstitial water of the present region are in the range 5.5–6 (Andersson et al., 2014). In the near vicinity of rusting meteoritic iron, pH conditions could, however, be significantly different, depending on the active corrosion mechanism. For example, hydrolysis in the presence of chloride anions promotes production of H^+ (Selwyn et al., 1999). In sample (B), akaganeite formed from direct oxidation of parahibbingite (similar to what has been observed for hibbingite [γ-$Fe_2(OH)_3Cl$] on anthropogenic iron; Simon et al., 2018), and it thus has a remarkably high Cl content.

https://doi.org/10.1180/mgm.2024.78 Published online by Cambridge University Press

Remarks on the current akaganeite formula

In light of our findings, a brief discussion around the formula of this mineral is necessary. The currently IMA-approved formula of akaganeite is $(Fe^{3+},Ni^{2+})_8(OH,O)_{16}Cl_{1.25}\cdot nH_2O$. Starting from the octahedral sites, the current formula involves Ni as an essential structural component. While it is true that some Ni can enter at the expense of Fe, it is well known that akaganeite does not require Ni to form: in fact, there are several examples of Ni-free akaganeite, both synthetic (*e.g.* Cai et al., 2001; Villalba et al., 2013) and natural (*e.g.* Mackay, 1962; Bibi et al., 2011). Furthermore, when present, Ni is disordered over Fe-dominant positions; for all the above reasons, it is not fundamental to display nickel in the formula. Even so, the presence of a divalent cation as a substituent for a trivalent cation implies different O/OH ratios to balance the charge; hence, at the end of this section, two formulae (with and without Ni) will be proposed.

Cl is located at a specific structural position, and it is then correctly indicated in the formula. However, we suggest that Cl should be reported as a range, because the amount of measured Cl in each sample can vary considerably, also having consequences on the amount of OH^- substituting for O^{2-} required to compensate the negative charge introduced by the chloride ion.

Based on all these considerations, the new proposed formulae could be written as $FeO_{1-x}(OH)_{1+x}Cl_x$ ($0.01 < x < 0.20$), or, taking Ni into account, $(Fe_{1-x}Ni_x)O_{1-x-y}(OH)_{1+x+y}Cl_y$ ($0 < x < 0.19$ and $0.01 < y < 0.20$), and $Z = 8$.

On the occurrence of humboldtine

Oxalate minerals are quite rare in nature, but occur in diverse environments (Echigo and Kimata, 2010); humboldtine from Muonionalusta could be the first

https://doi.org/10.1180/mgm.2024.78 Published online by Cambridge University Press

example related to terrestrial weathering of a meteorite (none reported by Rubin and Ma, 2017). Iron oxalate may form from direct reaction between oxalic acid and Fe minerals (*e.g.* Vehmaanperä et al., 2022). This is not a likely scenario for Muonionalusta, because there is no obvious source for the high concentrations necessary, and with the reaction kinetics expected in the present climate zone, it is not realistic. The high Ni content of the present mineral is not in line with a simple dissolution-precipitation mechanism either. Instead, interaction with organisms that can produce metal oxalate seems possible, like lichens or fungi (Gadd et al., 2014). For example, experimental work has shown that the ubiquitous fungus *Aspergillus niger* (blackmold) can accumulate both Fe and Ni, and excrete hydrated oxalates corresponding to humboldtine and andreybulakhite (Magyarosy et al., 2002; Zelenskaya et al., 2021).

Concluding statement

The conditions under which akaganeite forms commonly favour rapid nucleation, resulting in the simultaneous formation of many small crystals. This leads to competition for available iron, chlorine and oxygen, limiting the resources each crystal can access and thereby restricting their size. Moreover, the environments that facilitate akaganeite formation frequently offer only relatively short periods for growth, such as during specific stages of corrosion, which further prevents the development of large crystals. All these considerations make the discovery of large, well-developed akaganeite crystals unexpected and interesting.

Geochemical and mineralogical studies of mineral rust samples offer fundamental insights into both the terrestrial and extraterrestrial realms. The analysis of composition and transformation of rust in meteorite samples unravel the complex

https://doi.org/10.1180/mgm.2024.78 Published online by Cambridge University Press

interactions between cosmic materials and their environments.

Acknowledgements

Thanks are due to Andreas Forsberg, Johan Söderhielm and Anders Zetterqvist for providing Muonionalusta specimens over the years to the Swedish Museum of Natural History. Sigle-crystal X-ray data were collected at CRIST (Centro di Servizi di Cristallografia Strutturale), Università degli Studi di Firenze. The authors acknowledge P. Leverett and two anonymous referees for their feedback and suggestions, which have significantly improved the quality of this manuscript.

Competing interests: the authors declare none.

References

Andersson M., Carlsson M., Ladenberger A., Morris G., Sadeghi M. and Uhlbäck J. (2014) *Geochemical atlas of Sweden.* Elanders Sverige AB, Uppsala, 208 pp.

Biagioni C., Capalbo C. and Pasero M. (2013) Nomenclature tunings in the hollandite supergroup. *European Journal of Mineralogy*, **25**, 85-90.

Bibi I., Singh B. and Silvester E. (2011) Akaganéite (β-FeOOH) precipitation in inland acid sulfate soils of south-western New South Wales (NSW), Australia. *Geochimica et Cosmochimica Acta*, **75**, 6429-6438.

Bland P.A., Zolensky M.E., Benedix G.K. and Sephton M.A. (2006) Weathering of chondritic meteorites. Pp. 853-867 in: *Meteorites and the early solar system II* (D.S. Lauretta and H.Y. McSween, editors). University of Arizona Press, Tucson.

https://doi.org/10.1180/mgm.2024.78 Published online by Cambridge University Press

Blichert-Toft J., Moynier F., Lee C.T.A., Telouk P. and Albarède F. (2010) The early formation of the IVA iron meteorite parent body. *Earth and Planetary Science Letters*, **296**, 469-480.

Bruker (2016) *APEX3, SAINT and SADABS.* Bruker AXS Inc., Madison, Wisconsin, USA.

Buchwald V.F. (1975) *Handbook of iron meteorites. Their history, distribution, composition and structure.* University of California Press, Berkeley, 1426 pp.

Buchwald V.F. and Clarke R.S. (1989) Corrosion of Fe-Ni alloys by Cl-containing akaganeite (β-FeOOH); the Antarctic meteorite case. *American Mineralogist*, **74**, 656-667.

Cai J., Liu J., Gao Z., Navrotsky A. and Suib S.L. (2001) Synthesis and anion exchange of tunnel structure akaganeite. *Chemistry of Materials*, **13**, 4595-4602.

Cambier S.M., Verreault D. and Frankel G.S. (2014) Raman investigation of anodic undermining of coated steel during environmental exposure. *Corrosion*, **70**, 1219-1229.

de la Fuente D., Díaz I., Simancas J., Chico B. and Morcillo M.J.C.S. (2011) Long-term atmospheric corrosion of mild steel. *Corrosion Science*, **53**, 604-617.

Echigo T. and Kimata M. (2008) Single-crystal X-ray diffraction and spectroscopic studies on humboldtine and lindbergite: weak Jahn–Teller effect of Fe^{2+} ion. *Physics and Chemistry of Minerals*, **35**, 467-475.

Echigo T. and Kimata M. (2010) Crystal chemistry and genesis of organic minerals: a review of oxalate and polycyclic aromatic hydrocarbon minerals. *The Canadian Mineralogist*, **48**, 1329-1357.

https://doi.org/10.1180/mgm.2024.78 Published online by Cambridge University Press

Fagerlind T. (1981) *Glacial development in the Pajala district of northern Sweden.* Sveriges geologiska undersökning BA 27, Uppsala, 118 pp.

Fu X., Jia L., Wang A., Cao H., Ling Z., Liu C., Shi E., Wu Z., Li B. and Zhang J. (2020) Thermal stability of akaganeite and its desiccation process under conditions relevant to Mars. *Icarus*, **336**, 113435.

Gadd G. M., Bahri-Esfahani J., Li Q., Rhee Y.J., Wei Z., Fomina M. and Liang X. (2014) Oxalate production by fungi: significance in geomycology, biodeterioration and bioremediation. *Fungal Biology Reviews*, **28**, 36-55.

Giester G., Rieck B., Lengauer C. L., Kolitsch U. and Nasdala L. (2023) Katsarosite $Zn(C_2O_4)\cdot 2H_2O$, a new humboldtine-group mineral from the Lavrion Mining District, Greece. *Mineralogy and Petrology*, **117**, 259-267.

Gurdziel A. (2012) Wietrzenie meteorytu Muonionalusta. *Acta Societatis Metheoriticae Polonorum*, **3**, 30-38 (in Polish).

Hättestrand C. (2009) Sprängd dvärgplanet i nordsvensk myrmark. *Forskning och framsteg*, **3**, 46-51 (in Swedish).

Hidaka Y., Shirai N., Yamaguchi A. and Ebihara M. (2019) Siderophile element characteristics of acapulcoite–lodranites and winonaites: Implications for the early differentiation processes of their parent bodies. *Meteoritics & Planetary Science*, **54**, 1153-1166.

Holtstam D., Broman C., Söderhielm J. and Zetterqvist A. (2003) First discovery of stishovite in an iron meteorite. *Meteoritics & Planetary Science*, **38**, 1579-1583.

Holtstam D. and Söderhielm J. (2004) The Muonionalusta iron meteorites from Lapland, Sweden: New finds and findings. 5th International Conference "Mineralogy & Museums", Paris. *Bulletin de Liaison de la Société Française*

https://doi.org/10.1180/mgm.2024.78 Published online by Cambridge University Press

de Minéralogie et Cristallographie, **16**(2), 47.

Holtstam D. (2006) Akaganéite as a corrosion product of natural, non-meteoritic iron from Qeqertarsuaq, West Greenland. *GFF*, **128**, 69-71.

Holtstam D., Bindi L., Karlsson A., Söderhielm J. and Zetterqvist A. (2021) Muonionalustaite, $Ni_3(OH)_4Cl_2 \cdot 4H_2O$, a new mineral formed by terrestrial weathering of the Muonionalusta iron (IVA) meteorite, Pajala, Norrbotten, Sweden. *GFF*, **143**, 1-7.

Ladenberger A., Andersson M., Gonzalez J., Lax K., Carlsson M., Ohlsson S.Å and Jelinek, C. (2012) Markgeokemiska kartan. Morängeokemi i norra Norrbotten. *Sveriges geologiska undersökning*, **K410**, 1-112.

Lagerbäck R. and Wickman F.E. (1997) A new iron meteorite from Muonionalusta, northernmost Sweden. *GFF*, **119**, 193-198.

Li S. and Hihara L.H. (2015) A micro-Raman spectroscopic study of marine atmospheric corrosion of carbon steel: the effect of akaganeite. *Journal of the Electrochemical Society*, **162**, C495.

Libowitzky E. (1999) Correlation of OH stretching frequencies and OH···O hydrogen bond lengths in minerals. *Monatshefte fûr Chemie*, **130**, 1047-1059.

Mackay A.L. (1962) β-Ferric oxyhydroxide – akaganeite. *Mineralogical Magazine and Journal of the Mineralogical Society*, **33**, 270-280.

Magyarosy A., Laidlaw R., Kilaas R., Echer C., Clark D. and Keasling J. (2002) Nickel accumulation and nickel oxalate precipitation by *Aspergillus niger*. *Applied Microbiology and Biotechnology*, **59**, 382-388.

Margheri S., Bindi L., Bonazzi P. and Holtstam D. (2022) Structural and spectroscopic study of well-developed crystals of parahibbingite, β-$Fe_2(OH)_3Cl$, formed from terrestrial weathering of the Muonionalusta iron

https://doi.org/10.1180/mgm.2024.78 Published online by Cambridge University Press

meteorite. *Mineralogical Magazine*, **86**, 891-896.

Momma K. and Izumi F. (2011) VESTA 3 for three-dimensional visualization of crystal, volumetric and morphology data. *Journal of Applied Crystallography*, **44**, 1272-1276.

Murad E. and Bishop J.L. (2000) The infrared spectrum of synthetic akaganéite, β-FeOOH. *American Mineralogist*, **85**, 716-721.

Oh S.J., Cook D.C. and Townsend H. E. (1998) Characterization of iron oxides commonly formed as corrosion products on steel. *Hyperfine interactions*, **112**, 59-66.

Peretyazhko T.S., Ming D.W., Rampe E.B., Morris R.V. and Agresti D.G. (2018) Effect of solution pH and chloride concentration on akaganeite precipitation: Implications for akaganeite formation on Mars. *Journal of Geophysical Research: Planets*, **123**, 2211-2222.

Peretyazhko T.S., Pan M.J., Ming D.W., Rampe E.B., Morris R.V. and Agresti D.G. (2019) Reaction of akaganeite with Mars-relevant anions. *ACS Earth and Space Chemistry*, **3**, 314-323.

Post J.E. and Buchwald V.F. (1991) Crystal structure refinement of akaganéite. *American Mineralogist*, **76**, 272-277.

Post J.E., von Dreele R.B. and Buseck P.R. (1982) Symmetry and cation displacements in hollandites: Structure refinements of hollandite, cryptomelane and priderite. *Acta Crystallographica*, **B38**, 1056-1065.

Post J.E., Heaney P.J., von Dreele R.B. and Hanson J.C. (2003) Neutron and temperature-resolved synchrotron X-ray powder diffraction study of akaganéite. *American Mineralogist*, **88**, 782-788.

Rémazeilles C. and Refait P. (2007) On the formation of β-FeOOH (akaganéite)

https://doi.org/10.1180/mgm.2024.78 Published online by Cambridge University Press

in chloride-containing environments. *Corrosion Science*, **49**, 844-857.

Rubin A.E. and Ma C. (2017) Meteoritic minerals and their origins. *Geochemistry*, **77**, 325-385.

Selwyn L.S., Sirois P.I. and Argyropoulos V. (1999) The corrosion of excavated archaeological iron with details on weeping and akaganeite. *Studies in Conservationi*, **44**, 217-232.

Shebanova O.N. and Lazor P. (2003) Raman study of magnetite (Fe_3O_4): Laser-induced thermal effects and oxidation. *Journal of Raman Spectroscopy*, **34**, 845-852.

Sheldrick G.M. (2015) Structure refinement with SHELXL. *Acta Crystallographica*, **C71**, 3-8.

Simon H., Cibin G., Robbins P., Day S., Tang C., Freestone I. and Schofield E. (2018) A Synchrotron-based Study of the Mary Rose iron cannonballs. *Angewandte Chemie*, **130**, 7512-7517.

Song X. and Boily J.F. (2012) Variable hydrogen bond strength in akaganéite. *The Journal of Physical Chemistry C*, **116**, 2303-2312.

Ståhl K., Nielsen K., Jiang J., Lebech B., Hanson J.C., Norby P. and van Lanschot J. (2003) On the akaganéite crystal structure, phase transformations and possible role in post-excavational corrosion of iron artifacts. *Corrosion science*, **45**, 2563-2575.

Vehmaanperä P., Sihvonen T., Salmimies R. and Häkkinen A. (2022) Dissolution of magnetite and hematite in mixtures of oxalic and nitric acid: Mechanisms and kinetics. *Minerals*, **12**, 560.

Villalba J.C., Berezoski S., de Almeida Cavicchiolli K., Galvani V. and Anaissi F.J. (2013) Structural refinement and morphology of synthetic akaganéite

https://doi.org/10.1180/mgm.2024.78 Published online by Cambridge University Press

crystals, [β-FeO(OH)]. *Materials Letters*, **104**, 17-20.

Wickman F.E. (1964) The Muonionalusta iron meteorites. *Arkiv för mineralogi och geologi*, **3**, 467-478.

Wilson A.J.C. (1992) *International Tables for Crystallography. Volume C: Mathematical, Physical and Chemical Tables.* Kluwer Academic Publishers, Amsterdam.

Yew Y.P., Shameli K., Miyake M., Khairudin N.B.B.A., Mohamad S.E.B., Hara H., Nordin M.F.B.M. and Lee K.X. (2017) An eco-friendly means of biosynthesis of superparamagnetic magnetite nanoparticles via marine polymer. *IEEE Transactions on Nanotechnology*, **16**, 1047-1052.

Zelenskaya M.S., Izatulina A.R., Frank-Kamenetskaya O.V. and Vlasov D.Y. (2021) Iron oxalate humboldtine crystallization by fungus *Aspergillus niger*. *Crystals*, **11**, 1591.

https://doi.org/10.1180/mgm.2024.78 Published online by Cambridge University Press

Table headings

Table 1. Crystal data and SC-XRD experimental details.

Table 2. Atomic coordinates in the crystal structure of akaganeite.

Table 3. Selected interatomic distances (Å) for akaganeite.

Table 1. Crystal data and SC-XRD experimental details.

crystal-chemical formula	$Fe_8(O,OH)_{16}Cl_{0.984}$
Temperature (K)	293
a (Å)	10.560(4)
b (Å)	3.0268(12)
c (Å)	10.512(4)
β (°)	90.050(15)
V (Å^3)	336.0(2)
Z	8
crystal size (mm)	0.40 × 0.15 × 0.04
θ_{max} (Mo*K*α)	33.1°
R_{int} (%)	9.34
independent reflections	746
observed reflections [$F_o > 4\sigma(F_o)$]	711
refined parameters	42
wR_2* (%)	5.04
$R1_{all}$ (%)	2.31
$R1_{obs}$ (%)	2.23
GooF	1.028
$\Delta\rho_{max}$, $\Delta\rho_{min}$ (e$^-$/Å^3)	0.34, –1.73

*$w = 1/[\sigma^2(F_o^2) + (0.0381*P)^2]$ where $P = (F_o^2 + 2F_c^2)/3$

https://doi.org/10.1180/mgm.2024.78 Published online by Cambridge University Press

Table 2. Atomic coordinates in the crystal structure of akaganeite.

	x	*y*	*z*
Fe1	0.85655(4)	0	0.34261(3)
Fe2	0.34366(4)	0	0.14201(4)
O1	0.6554(1)	0	0.2966(1)
O2	0.6648(2)	0	0.0424(2)
O3	0.2875(2)	0	0.3446(2)
O4	0.0413(2)	0	0.3424(1)
Cl	0	0	0

Table 3. Selected interatomic distances (Å) for akaganeite.

Fe1–O2 (x2)	1.950(1)	Fe2–O2	1.941(2)
–O4	1.951(2)	–O4 (x2)	1.947(1)
–O1 (x2)	2.109(1)	–O3 (x2)	2.057(1)
–O1'	2.178(2)	–O3'	2.211(2)
<Fe1–O>	2.041	<Fe2–O>	2.027
O1–O2	2.674(3)	O2–O3 (x2)	2.881(3)
–O1 (x2)	2.692(3)	–O4 (x2)	2.899(3)
–O4 (x2)	2.956(3)	–O4' (x2)	2.915(3)
–O2' (x2)	2.958(3)	–O2 (x2)	3.027(1)
–O1' (x2)	3.027(1)	–Cl (x2)	3.568(3)
–Cl (x2)	3.092(2)		
O3–O4	2.600(3)	O4–O4 (x2)	3.027(1)
–O3 (x2)	2.621(3)	–Cl (x2)	3.625(3)
–O3' (x2)	3.027(1)		
–O4' (x2)	3.070(3)		
–Cl (x2)	3.160(2)	Cl–Cl (x2)	3.027(1)

https://doi.org/10.1180/mgm.2024.78 Published online by Cambridge University Press

Figure captions

Figure 1. (a–b) Colour images of akaganeite crystals. Sample GEO-NRM #20040065.

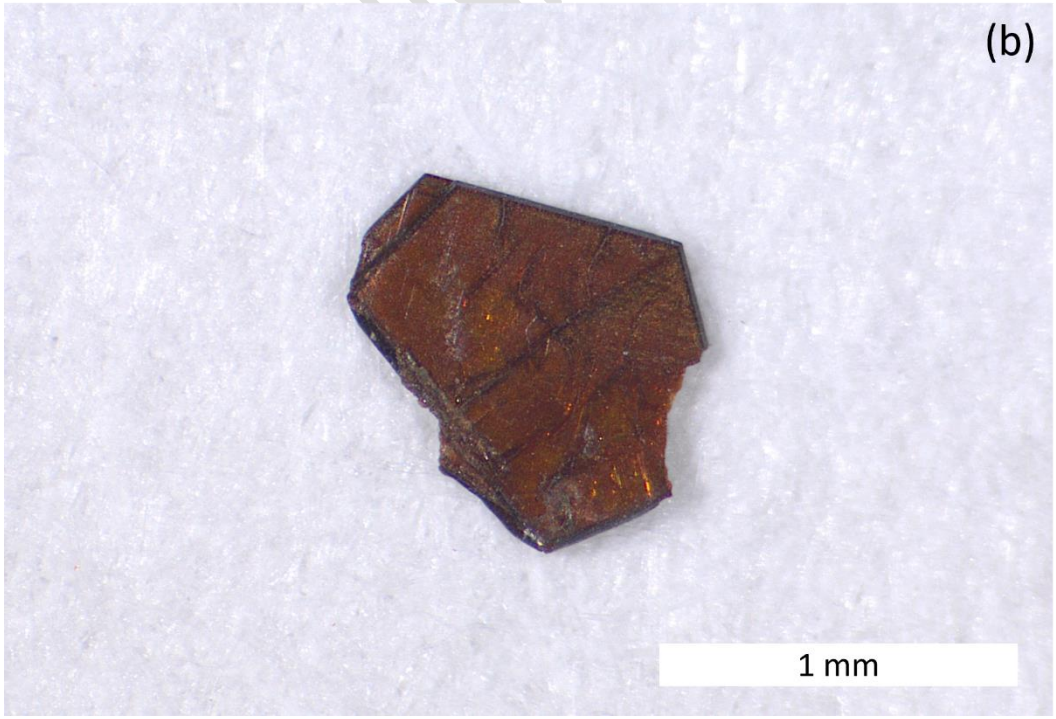

https://doi.org/10.1180/mgm.2024.78 Published online by Cambridge University Press

Figure 2. Colour image of a cavity with akaganeite crystals and dark brown, botryoidal goethite. Sample GEO-NRM #20040065.

Figure 3. SEM image of akaganeite forming a rim on parahibbingite. Sample GEO-NRM #20060957.

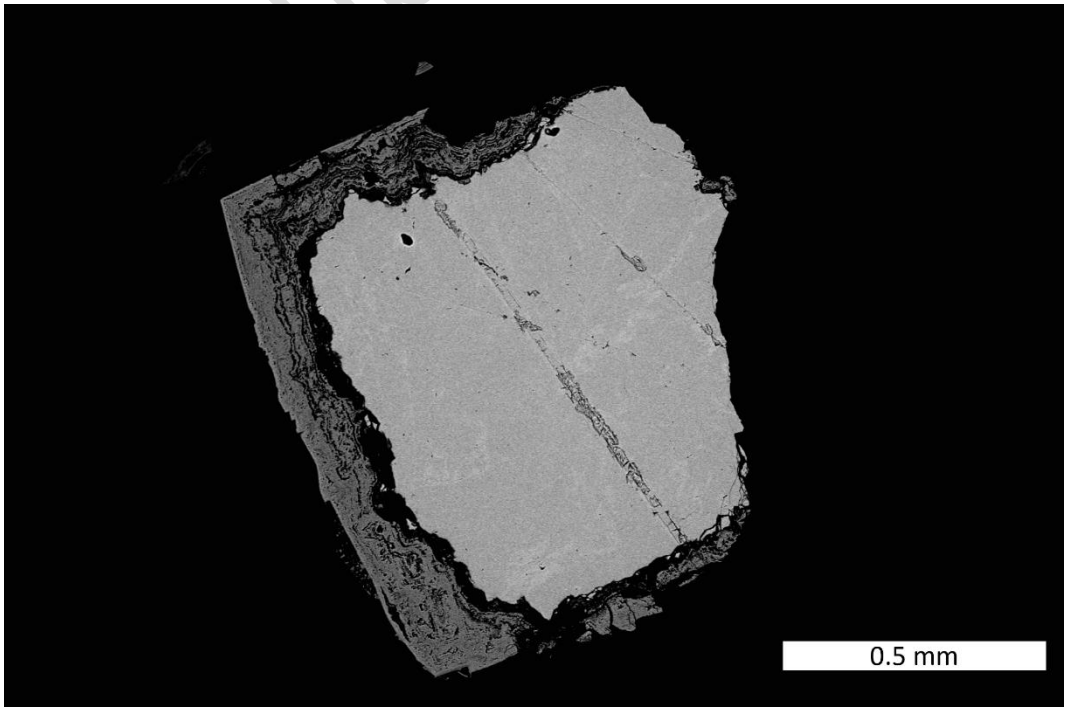

https://doi.org/10.1180/mgm.2024.78 Published online by Cambridge University Press

Figure 4. Raman spectrum of akaganeite. Sample GEO-NRM #20060957.

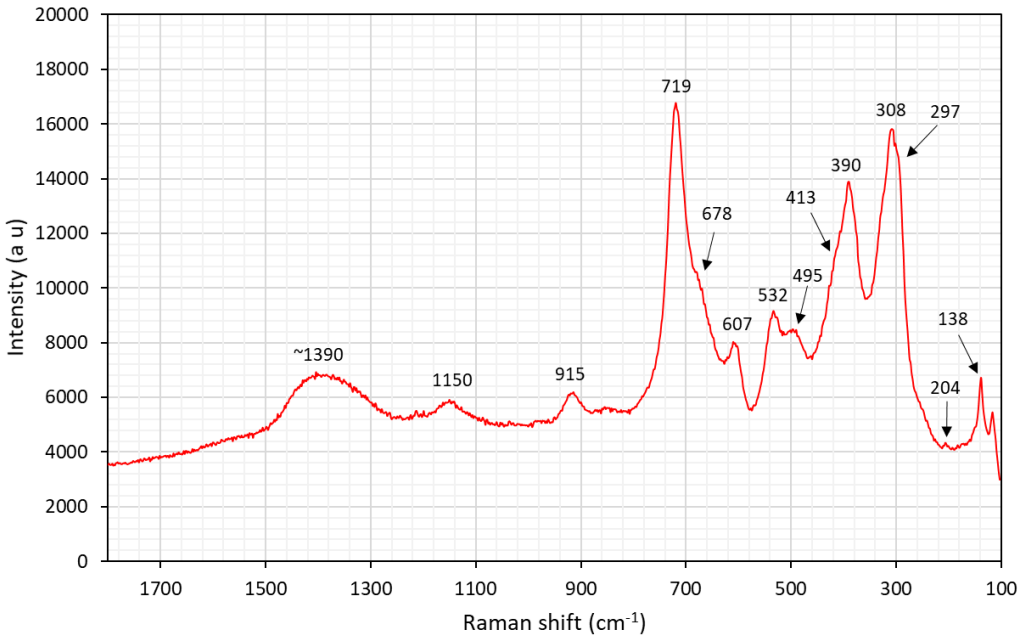

Figure 5. Raman spectrum of laser-transformed akaganeite.

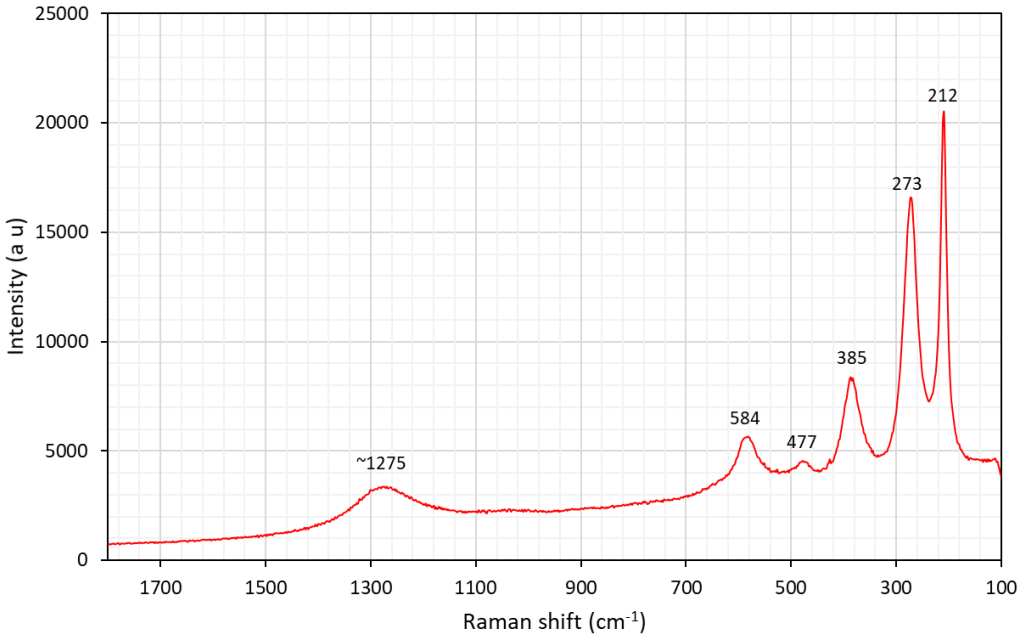

https://doi.org/10.1180/mgm.2024.78 Published online by Cambridge University Press

Figure 6. Colour image of yellowish humboldtine aggregate. Black spherical grains are poorly crystalline goethite. Sample GEO-NRM #20050170.

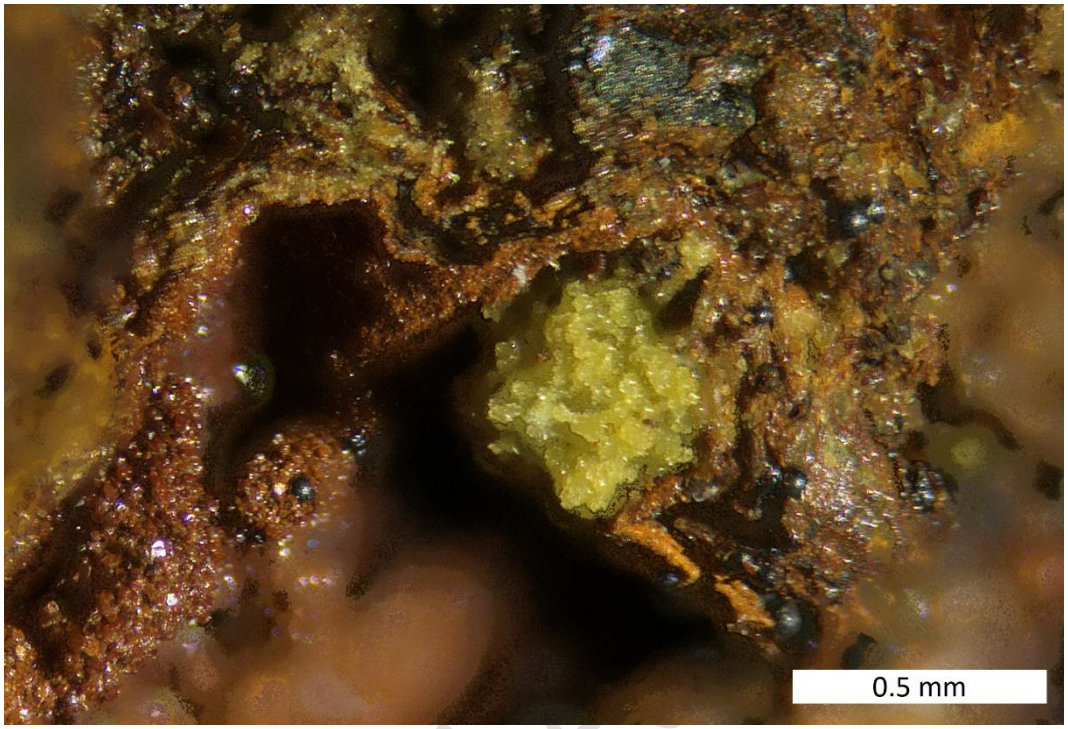

Figure 7. Raman spectrum of humboldtine. Sample GEO-NRM #20050170.

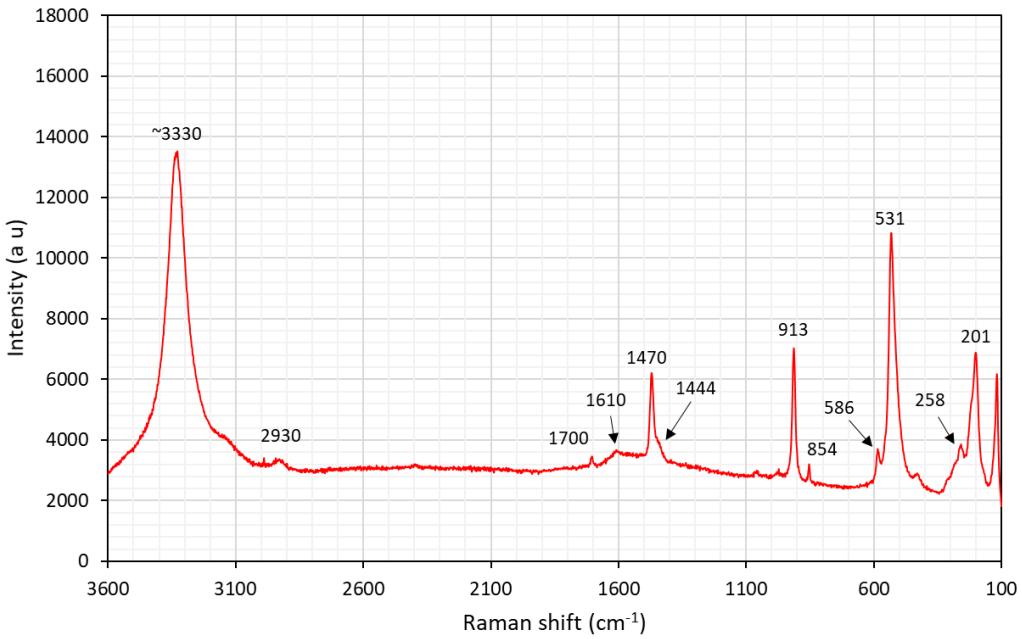

https://doi.org/10.1180/mgm.2024.78 Published online by Cambridge University Press

Figure 8. Projection of the akaganeite structure approximately down the [010] axis. The green spheres at the centre of the tunnel represent chloride ions. The structure was drawn using VESTA (Momma and Izumi, 2011).

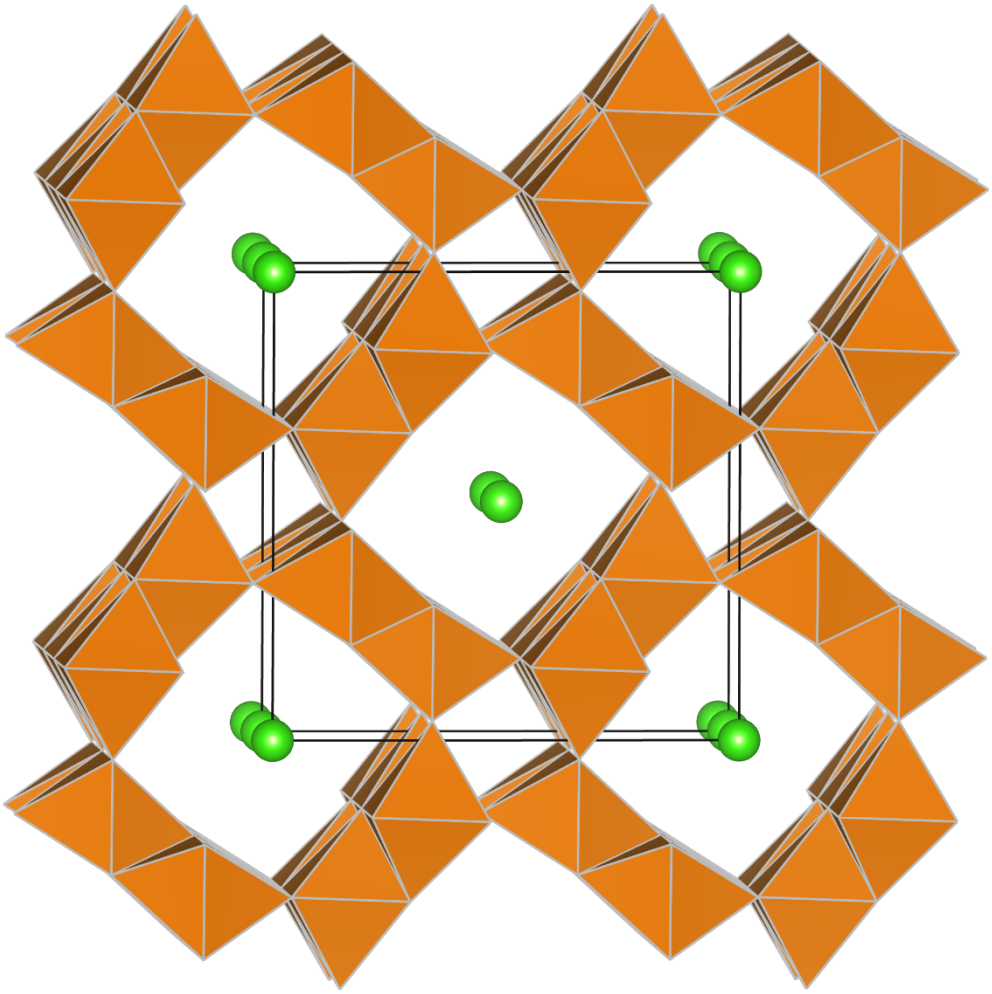

https://doi.org/10.1180/mgm.2024.78 Published online by Cambridge University Press